LBL-11125
Preprint

Lawrence Berkeley Laboratory
UNIVERSITY OF CALIFORNIA

Materials & Molecular Research Division

Submitted to the Journal of Materials Science

GASEOUS REDUCTION OF AN ALLOY OXIDE

Jeffrey S. Allender and Lutgard C. De Jonghe

September 1980

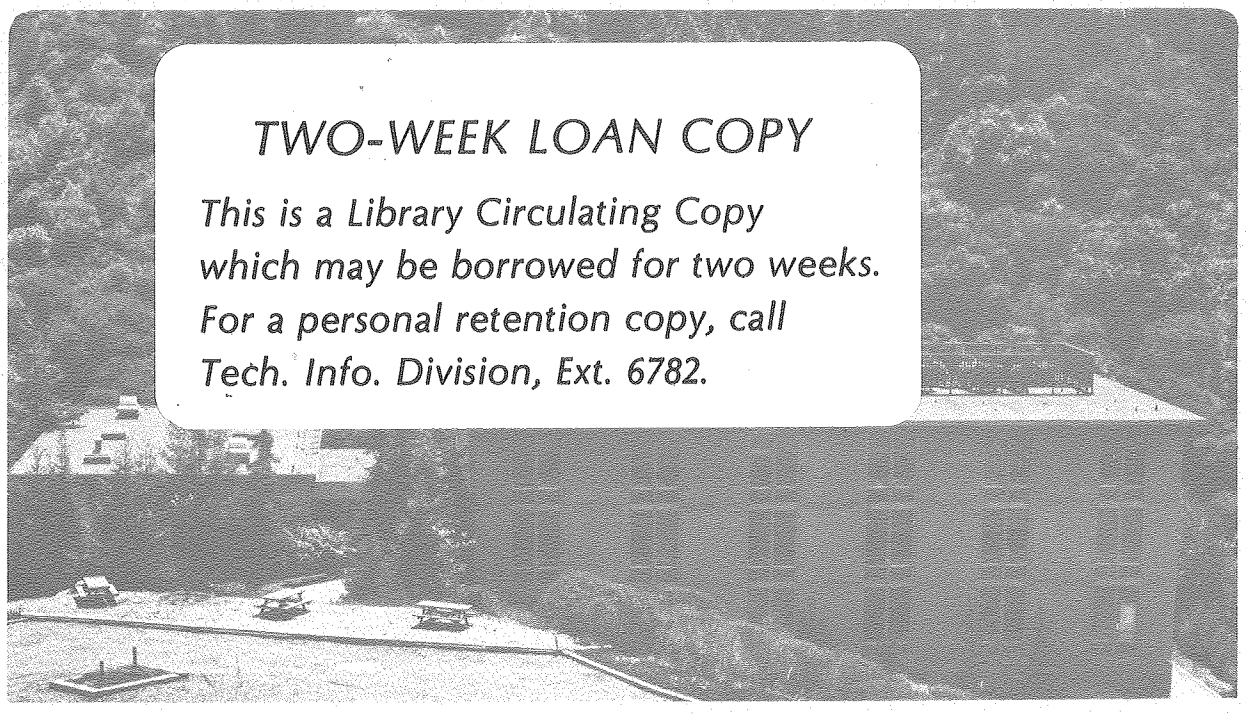

Prepared for the U.S. Department of Energy under Contract W-7405-ENG-48

DISCLAIMER

GASEOUS REDUCTION OF AN ALLOY OXIDE

September, 1980

Jeffrey S. Allender
Savannah River Laboratory
E.I. duPont de Nemours Co., Inc.
Aiken, South Carolina 29801

Lutgard C. De Jonghe
Materials and Molecular Research Division
Lawrence Berkeley Laboratory

and

Department of Materials Science and Mineral Engineering
University of California
Berkeley, California 94720

GASEOUS REDUCTION OF AN ALLOY OXIDE

Jeffrey S. Allender
Savannah River Laboratory
E.I. duPont de Nemours Co., Inc.
Aiken, South Carolina 29801

Lutgard C. De Jonghe
Materials and Molecular Research Division
Lawrence Berkeley Laboratory
and
Department of Materials Science and Mineral Engineering
University of California
Berkeley, California 94720

ABSTRACT

$Ni(Al,Fe)_2O_4$ ceramic alloys were reduced by hydrogen gas at 1 atm, between 450°C and 800°C. The reaction rate was determined from the rate of advance of the porous metal product layer/unreduced oxide interface. A simple analysis was presented permitting assessment of the interface reaction resistance and the gas transport resistant through the porous product scales. The reaction was under mixed control in all conditions studied. In a range of temperatures and reaction times, preferred grain boundary attack was observed. The conditions under which this was observed depended strongly on the Al^{3+} content of the ceramic alloy. Al^{3+} also lowered the interface reaction rate and inhibited scale coarsening by formation of dispersed unreduced phases in the product scales.

I. Introduction

When a dense oxide alloy reacts with a strongly reducing gas such as hydrogen, a porous metal product layer can develop at its surface. If the gas flow is sufficient to eliminate the external mass transfer resistance, the pore structure of the metal layer and the nature of the metal/oxide interface reaction will determine the overall reaction rate kinetics. When the reduction is directly from dense unreduced oxide to metal alloy and the reaction is topochemical, a fairly simple reduction model may be applied [1,2]. This model leads to layer growth kinetics described by

$$\dot{\xi} = \frac{p^o_{H_2}}{RTC_o} \left(\frac{\xi}{D_{eff}} + \frac{1}{k_r} \right)^{-1} \qquad (1)$$

where ξ = porous product layer thickness (cm)

$\dot{\xi}$ = $d\xi/dt$ (cm/sec)

$p^o_{H_2}$ = hydrogen pressure in the gas stream (atm)

R = gas constant (atm cm^3/mole K)

T = temperature (K)

C_o = oxygen concentration in the solid oxide (g-atom O/cm^3)

D_{eff} = effective gas diffusivity in the porous product layer (cm^2/sec)

k_r = interface reaction rate parameter (cm/sec).

The details of the assumptions involved in this model have been discussed by Porter and De Jonghe [2]. The form of Eq. (1) is similar to the one developed first by Evans in 1924 [3] to describe the influence of the interface reaction on oxidation.

Analysis of the layer growth data with Eq. (1) will thus permit a separation of the contributions to the overall reaction resistance of gas diffusion in the scale and of the interface reaction. This rate equation was used recently to study the details of the reduction reaction of cobalt ferrite [2]. The effects on the kinetics of substitutionally alloying the cobalt ferrite with aluminum were recently reported by Rey and De Jonghe [4]. It appeared that in certain temperature ranges hard-to-reduce ions such as Al^{3+} promote extensive grain boundary reduction, and can inhibit pore coarsening in the product scale.

In this paper we report on the reduction kinetics and product phase morphologies of $NiFe_2O_4$ and $Ni(Al,Fe)_2O_4$ ceramic alloys. Although Ni and Co are fairly similar elements, some interesting differences exist in the Ni-Fe-O and the Co-Fe-O phase relationships that should affect the kinetics and micromorphology of the reduction. Comparison of the phase diagrams of nickel-iron oxides [5] and of cobalt-iron oxides [6] in Fig. 1 shows that Ni is not significantly soluble in FeO, in contrast to Co, leading to different expected phases. In addition, Ni ions diffuse significantly slower than Co ions in their respective ferrite spinels at all oxygen activities [7].

II. Experimental Procedures

The alloy oxides were dense polycrystalline $NiFe_2O_4$, $NiAl_{0.02}Fe_{1.98}O_4$, and $NiAl_{0.1}Fe_{1.9}O_4$. Grain sizes were between 4 and 8 microns. Porosities were about 2.5 percent.

Cube-shaped samples of approximately 0.7 cm edge length were placed in a platinum wire basket in a flowing stream of hydrogen at 1 atm. The hydrogen gas contained less than 1 ppm of impurities. It was found that a flow rate of 2 cm sec^{-1} at the sample was sufficient to eliminate any dependence of reaction rate on mass transfer to or from the sample surface at all reaction temperatures. After partial reduction, the samples were withdrawn from the hot zone of the furnace and were rapidly cooled in flowing hydrogen. This procedure effectively quenched the samples in their high-temperature morphology and prevented partial reoxidation during cooling. Temperatures used in the reduction were 450°C, 500°C, 550°C, 600°C, 700°C, and 800°C.

After reaction, the partially reduced specimens were cross-sectioned and polished, and the total product layer thickness was determined by optical microscopy. The specimens were briefly etched in a 2N HCl solution and reexamined. The etching solution selectively attacked the (Fe,Ni)O phase when present, but did not affect metal-alloy or spinel phases. Although some local variation in the interface position occurred, the movement of the average bulk/scale interface was sufficiently topochemical to allow

determination of a scale thickness with less than a 5 percent error. The values reported for the scale thicknesses are averages from three to five replicate experiments. The pore structures of the product scales were examined with the scanning electron microscope.

III. Experimental Results and Discussions

3.1. Kinetic measurements

The results of the layer measurements are shown in Figs. 2-4. The product layer thicknesses after a reaction time of 3000 sec are compared in Fig. 5. For $NiFe_2O_4$ and $NiAl_{0.02}Fe_{1.98}O_4$, the increase of the interface advance rate diminishes in a temperature range between 500°C and 700°C. This slowdown is, however, not comparable to the pronounced reaction rate minimum that was observed for cobalt ferrites in this temperature range. For $NiAl_{0.1}Fe_{1.9}O_4$ alloys, a reaction rate slowdown is not observed. These results clearly demonstrate the pronounced effect of Al^{3+} on the reduction behavior of the Ni-Al-Fe oxide alloys.

To permit further analysis, Eq. (1) can be integrated to yield:

$$a\xi^2 + b\xi = t \qquad (2)$$

where

$$a = \frac{C_o RT}{2D_{eff}} \frac{1}{p^o_{H_2}} \tag{3}$$

$$b = \frac{C_o RT}{k_r} \frac{1}{p^o_{H_2}} \tag{4}$$

The form of Eq. (2) is similar to one used by Lu and Bitsianes [8].

Equation (2) can be further manipulated to yield

$$b/a = (t_2 \xi_1^2 - t_1 \xi_2^2)/(t_1 \xi_2 - t_2 \xi_1) \tag{5}$$

where the subscripts to t and ξ represent times t_1 and t_2. From Eq. (2) also follows:

$$a = t/(\xi^2 + b\xi/a) \tag{6}$$

Thus, from Eqs. (3)-(6), D_{eff} and k_r can be found. We also note that when

$$\xi = \xi_c \simeq b/2a \tag{7}$$

we have $\xi_c = D_{eff}/k_r$. At this product layer thickness, ξ_c, the gas diffusion resistance and the interface reaction

resistance contribute equally to the control of the overall reduction kinetics. Thus, the reaction will be mainly under interface reaction control when $\xi \ll b/2a = \xi_c$, and will be under gas transport control when $\xi \gg \xi_c$.

Application of this analysis to the data obtained for the reduction of nickel ferrites yielded the results shown in Table I.

Comparison of these values of ξ_c listed in Table I with the data plotted in Figs. 2-4 clearly indicates that the reactions are under mixed control in the temperature and time intervals of the measurements. In addition, for the measurement interval reported here, the importance of the gas transport resistance through the porous scale increases with increasing temperatures.

Calculated values of D_{eff} are shown in Fig. 6. D_{eff} for $NiFe_2O_4$ and $NiAl_{0.002}FE_{1.98}O_4$ does not vary simply with temperature. Below 500°C, D_{eff} decreases rapidly with decreasing temperatures, while above 500°C D_{eff} changes only little. Values above 500°C could not be obtained for these materials, since the microstructural examination of the scales, reported below, showed that the model underlying Eq. (1) was no longer valid. The values for D_{eff} for $NiAl_{0.02}Fe_{1.98}O_4$ were generally lower than those for $NiFe_2O_4$. It is interesting to compare the effective gas diffusion coefficients for the transport through the porous product layer, D_{eff}, for $NiFe_2O_4$ and for $CoFe_2O_4$ [3] at 600°C: $D_{eff} \simeq 0.005$ for nickel ferrites, while $D_{eff} \simeq 0.4$ for

cobalt ferrite. This difference implies significantly different pore structures for the product scales of these two materials.

The values of k_r for nickel aluminum ferrites are shown in Fig. 7. k_r appears to follow a simple Arrhennius relationship, suggesting that the same interface process occurred for the temperature domain in which Eq. (1) is valid. The activation enthalpy for k_r for $NiFe_2O_4$ and for $NiAl_{0.02}Fe_{1.98}O_4$ is 10 kcal/mole, while for $NiAl_{0.1}Fe_{1.98}O_4$ it is 12 kcal/mole. The main action of Al^{3+} alloying additions thus appears to be the depression of the preexponential factor of the interface reaction-rate parameter. This may be due to the formation of small iron aluminate precipitates at the reaction interface, so that the number of reaction sites accessible to the reducing gas is lowered. Formation of iron aluminate precipitates is to be expected, since they were also formed in the gaseous reduction of cobalt ferrites alloyed with Al^{3+} [3].

3.2 Micromorphology of the product layers

A range of microstructures was observed in the reaction product layers of the different alloy oxides. These microstructures are dependent upon temperature, composition, and reaction time. In general, at the lower reaction temperatures all scales consisted simply of a porous metal alloy. At temperatures above 600°C, the scales that formed on $NiFe_2O_4$ and on $NiAl_{0.02}Fe_{1.98}O_4$ were more complex and proved to be two-phase.

3.2.1. $NiFe_2O_4$

Up to about 600°C the metal product layers formed on this material were single phase and exhibited a clear reaction interface. At 600°C, i.e., above the (Fe,Ni)O stability temperature, a single-phase porous metal scale was formed initially, with a clear spinel/metal interface. However, after long reaction periods the metal phase formed preferentially along the original spinel boundaries, and unreduced oxide was partly retained. Etching showed that wüstite constituted a small fraction of the retained oxide. At 700°C, this two-phase scale was clearly established, and all the retained oxide was identified as wüstite except for a few isolated regions of a partially reduced nickel-deficient spinel directly at the unreduced oxide/reduced scale interface. A cross section of the product scale is shown in Fig. 8. It is expected that the phase diagram at this temperature and above is similar to the one shown in Fig. 1 for 1000°C. If wustite is formed, the scale must be two-phase for such a phase relationship. This is in contrast to $CoFe_2O_4$, where the phase diagram suggests the formation of a distinct single-phase (Co,Fe)O subscale. At 800°C the two-phase region of the scale is even more pronounced, as one would expect on the basis of the phase diagram.

A micrograph of an etched interface region after 1500 sec of reduction at 800°C is shown in Fig. 9. Two two-phase reaction layers can be observed: metal + spinel and metal + wüstite. The

sequence of phases at 800°C is therefore: unreduced spinel/spinel + metal/wüstite + metal/metal. At 800°C the reaction layer phase relationship corresponds to a vertical section through the $\ln p_{O_2}$-composition diagram, with the NiO-rich phase absent.

Clearly, above 600°C a single-phase, topochemical scale structure is no longer present, and the two-phase nature of the scale precludes the use of Eq. (1) to describe the reduction kinetics.

The evolution of the scale pore structure is shown in Fig. 10 for scales formed between 450°C and 600°C. At the lower temperature the pore structure is bimodal. The scale forms a very finely porous metallic relic of the original spinel grains, with coarse inter-relic pores, as shown in Fig. 11. With increasing reduction temperatures, the pores coarsen and the scale evolves to a more uniform structure. This pore structure evolution with increasing temperature causes the behavior of D_{eff} previously discussed.

3.2.2 $NiAl_{0.02}Fe_{1.9}O_4$

The microstructural aspects of the scales formed on this material are comparable to those of $NiFe_2O_4$. Up to 600°C, a single porous metal product layer is formed. Above 600°C, the microstructural sequence is again: spinel/spinel + metal/wüstite + metal/metal. There are some differences, however, from the $NiFe_2O_4$ behavior: even after 7000 sec reduction at 600°C the

structure is still spinel/metal. At 700°C the presence of Al^{3+} appears to have promoted preferential grain boundary attack after an initially well-defined interface was formed (Fig. 12). We believe that this behavior can be understood by considering the relative rates of the reaction interface advance and of the interface solid-state transport processes. When an alloy oxide is reduced, the less reducible ion will accumulate ahead of the advancing reaction interface. The degree of accumulation, and thus of the interface composition, depends on solid-state transport rates. Similar phenomena are found at the metal/scale interfaces in the oxidation of metal alloys (see e.g., Ref. 9). In the case of gaseous reduction, the interface velocity depends on the gas composition as well as on the interface composition. In a first approximation, the interface segregation phenomena and the interface velocity can be considered as independent. Then, when the ratio $\dot{\xi}/J_s$ of interface velocity to solid-state diffusion rate, J_s, is comparatively high, chemical polarization should develop quickly, while if $\dot{\xi}/J_s$ is comparatively low the chemical polarization would be less. Chemical polarization, i.e., buildup of Fe^{2+} in front of the advancing reaction interface, will slow the interface reaction rate. Preferential grain boundary reaction will then depend on the ratio D_{GB}/D_B of the grain boundary diffusivity to the grain bulk diffusivity, as well as on $\dot{\xi}/D_{GB}$. If the ratios $\dot{\xi}/D_{GB}$ and $\dot{\xi}/D_B$ are both comparatively high, chemical

polarization occurs rapidly everywhere and a simple interface should be observed. The condition for preferred grain boundary attack is then that ℓ / D_{GB} be low and D_{GB}/D_B be high. We can therefore expect alloy oxides to have a limited range of reaction conditions where grain boundary attack is pronounced. The location of this regime depends on kinetic parameters that are usually not known a priori.

3.2.3 $NiAl_{0.1}Fe_{1.9}O_4$

In this material, a simple spinel/metal structure was observed for all the reaction conditions studied. As in the case of reduction of $CoAl_{0.1}Fe_{1.9}O_4$ [3], the aluminum led to the formation of unreduced oxide particles, dispersed through the metal alloy, that strongly inhibited pore coarsening. The strong grain boundary attack that was observed for the Al^{3+}-alloyed cobalt ferrites was, however, not found for the alloyed nickel ferrites. This difference in behavior can be described as in the preceding section: ℓ / D_{GB} is relatively high under these test conditions, while D_{GB}/D_B is relatively low. As previously reported, significant grain boundary attack was indeed observed in the reduction of $NiAl_{0.1}Fe_{1.9}O_4$ in flowing Ar-5 percent H_2 at 1000°C [10].

IV. Conclusions

1. A simple analysis was presented permitting assessment of the interface reaction resistance and the gas transport resistance

through the scale for a topochemical reduction reaction.

2. $Ni(Al,Fe)_2O_4$ ceramic alloy oxides exhibited mixed reduction reaction control between 450°C and 800°C, at 1 atm of hydrogen. The gas transport resistance in the porous product layer increased in relative importance with increasing temperatures, in the measurement interval.

3. In a range of temperature and reaction times, preferred grain boundary reduction was observed. The conditions under which this grain boundary attack appeared depended strongly on the Al^{3+} content of the $Ni(Al,Fe)_2O_4$. This could be attributed to chemical polarization ahead of the advancing reaction interface. The extent of the chemical polarization depends on the relative magnitudes of the reaction interface velocity and the solid-state diffusion rates.

4. The phase relationships led to the formation of a two-phase scale when (Fe,Ni)O was present.

5. As in the reduction of $Co(Al,Fe)O_4$, the presence of Al^{3+} lowered the interface reaction rate and inhibited the scale coarsening.

V. Acknowledgments

D.P. Whittle is thanked for many stimulating discussions. M. Chang assisted in the microstructural observations.

A significant part of this work was carried out at Cornell University under DOE Contract EY-76-5-02-2584. Part of this work was also supported by the Basic Sciences Division of the U.S. Department of Energy under Contract W-7405-Eng-48.

VI. References

1. R.H. Spitzer, F.S. Manning, and W.O. Philbrook, Trans. Met. Soc. AIME, 236 (1966) 726.
2. J.R. Porter and L.C. De Jonghe, Met. Trans., accepted for publication, 1980.
3. U.R. Evans, Trans. Electrochem. Soc. 46 (1924) 247.
4. M.C. Rey and L.C. De Jonghe, J. Mat. Sci. in press, 1980.
5. J. Sticher and H. Schmalzried, Report, Inst. Theor. Huttenkunde, Tech. Univ. Claustahl, May 1975.
6. Calculated by Manlabs, Inc., 21 Erie Street, Cambridge, Massachusetts 02139.
7. R. Dieckmann, T.O. Mason, J.D. Hodge, and H. Schmalzried, Ber. Bunsenger. Phys. Chem. 82 (1978) 778.
8. W.-K. Lu and G. Bitsianes, Trans. Met. Soc. AIME, 236 (1966) 531.
9. C. Wagner, Corrosion Sci. 9 (1969) 91.
10. J. Allender and L.C. De Jonghe, in Ceramic microstructures '76, ed. R.M. Fulrath and J.A. Pask, Westview Press, Boulder, Colorado, 1977, pp. 556.

TABLE I. Product layer thickness, ξ_c, at which the gas diffusion and the interface reaction contribute equally to the total reaction resistance.

	ξ_c(mm)					
Material	450°C	500°C	550°C	600°C	700°C	800°C
$NiFe_2O_4$	0.4	0.45	0.19	0.13	-	-
$NiAl_{0.02}Fe_{1.98}O_4$	0.21	0.36	0.25	0.17	-	-
$NiAl_{0.1}Fe_{1.9}O_4$	-	0.06	0.07	0.04	0.13	0.24

Figure Captions

Fig. 1. a. Oxygen activity versus composition diagram for nickel ferrites at 1000°C [5]. XBL 807 1524

b. Oxygen activity versus composition diagram for cobalt ferrite [6]. The (Co,Fe)O and the (Ni,Fe)O fields have been shaded. XBL 807 1523

Fig. 2. Total product layer thickness, ξ, as a function of time and temperature for hydrogen reduction of $NiFe_2O_4$. XBL 807 1525

Fig. 3. Total product layer thickness, ξ, as a function of time and temperature for hydrogen reduction of $NiAl_{0.02}Fe_{1.98}O_4$. XBL 807 1521

Fig. 4. Total product layer thickness, ξ, as a function of time and temperature for hydrogen reduction of $NiAl_{0.1}Fe_{1.9}O_4$. XBL 807 1526

Fig. 5. Total product layer thickness, ξ, after 3000 sec as a function of temperature, T (°C), for reduction with hydrogen. XBL 807 1527

Fig. 6. The effective gas diffusion coefficient, D_{eff}, for transport through the porous product layer. Above 600°C the values of D_{eff} for $NiFef_2O_4$ and $NiAl_{0.02}Fe_{1.98}O_4$ could not be calculated since the scales were no longer single phase. XBL 807 1522

Fig. 7. The interface reaction rate parameter, k_r, as a function of temperature for nickel aluminum ferrite by hydrogen. XBL 807 1528

Fig. 8. Sequences of optical micrographs of scale cross section for $NiFe_2O_4$ reacted with hydrogen at 700°C for 5000 sec. a: interface, d: surface. P: pore (due to pullout on polishing), S: unreduced spinel, M: porous metal alloy, W: (Ni,Fe)O. The total scale thickness is about 3 mm. XBB 808 9666

Fig. 9. Optical micrograph of etched interface region of $NiFe_2O_4$ after 1500 sec of reduction at 800°C by hydrogen. Two two-phase reaction layers can be observed: M + W and M + S. M: porous metal alloy, S: spinel, W: (Ni,Fe)O, P: pore-pullout. XBB 808 9663

Fig. 10. Scanning electron micrographs of surfaces of porous metal product layers on $NiFe_2O_4$ reduced at a:450°C, b:500°C, c:550°C, d:600°C. At the lower temperatures the porous metal forms a relic of the original spinel grains. CBB 808 9665

Fig. 11. Scanning electron micrograph of cross section of metal scale formed on $NiFe_2O_4$ at 450°C. M: porous metal alloy, S: spinel. The pore structure in the scale is bimodal: coarse inter-relic pores and very fine relic pores. The surface of the scale is marked sur, the interface is located between M and S. XBB 808 9664

Fig., 12. Preferential intergranular reduction in $NiAl_{0.02}Fe_{1.98}O_4$ after 7000 sec of reduction at 600°C. M: porous metal alloy, S: spinel. XBB 808 9667

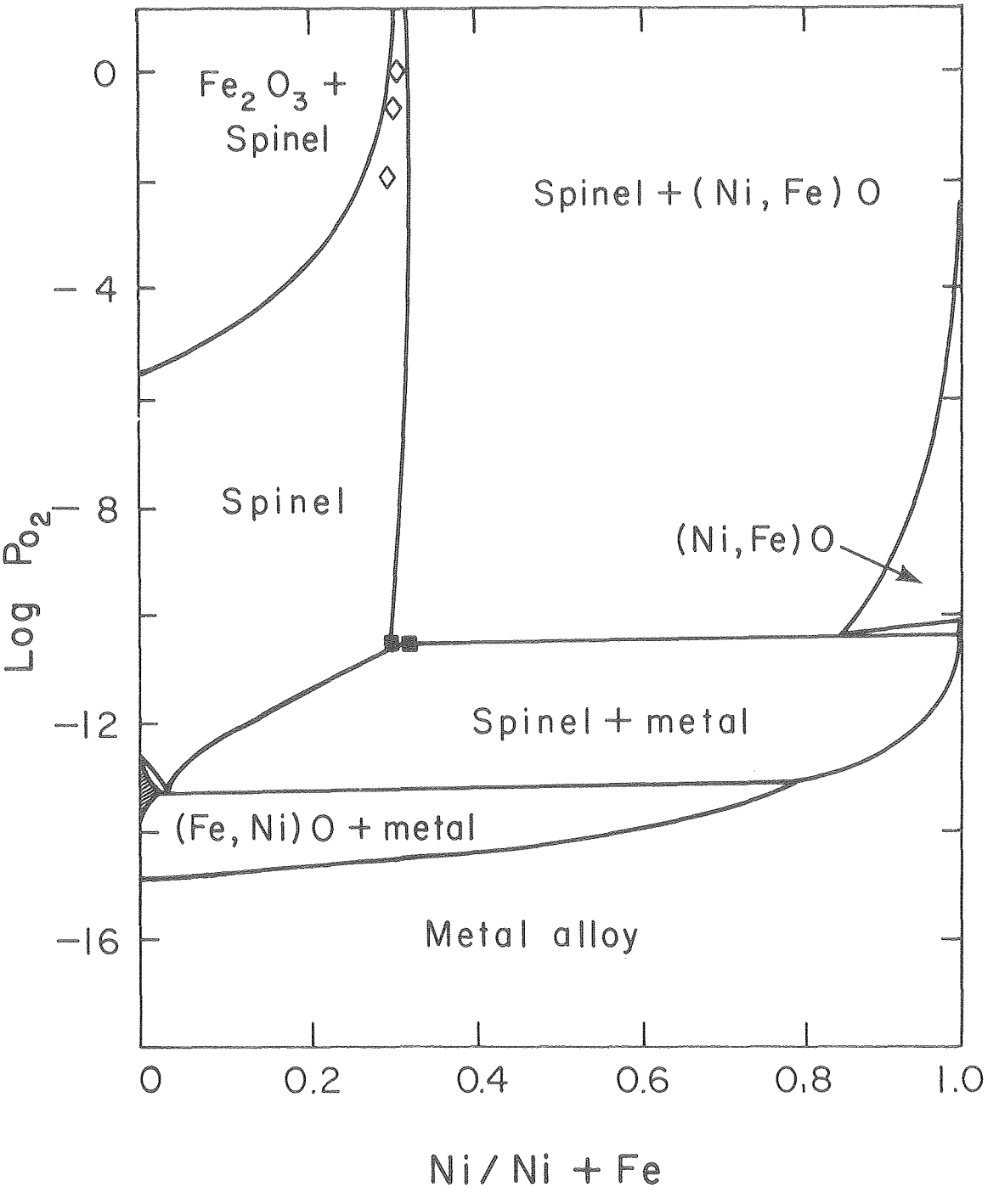

Figure 1 a

XBL 807-1524

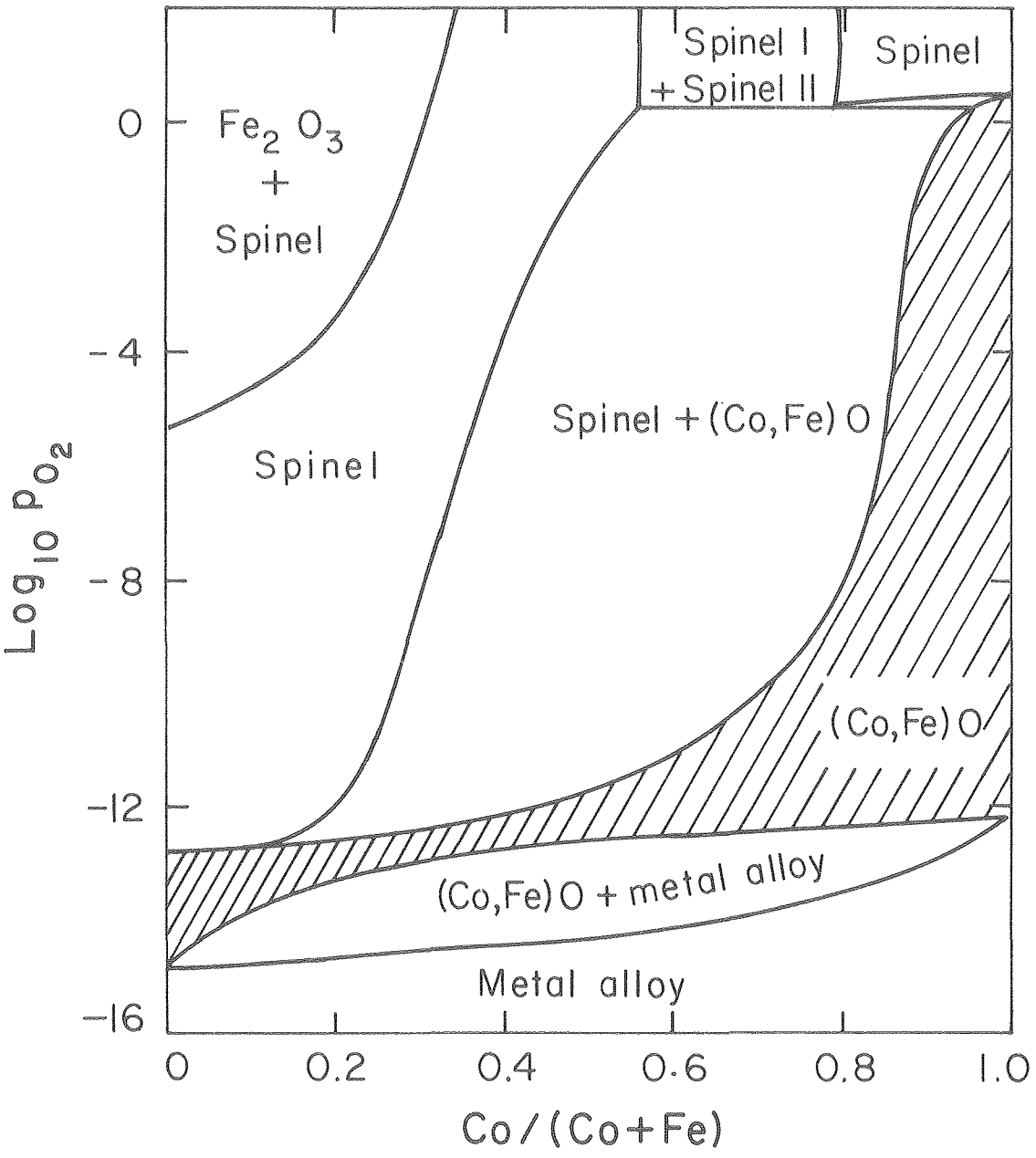

Figure 1 b

XBL 807-1523

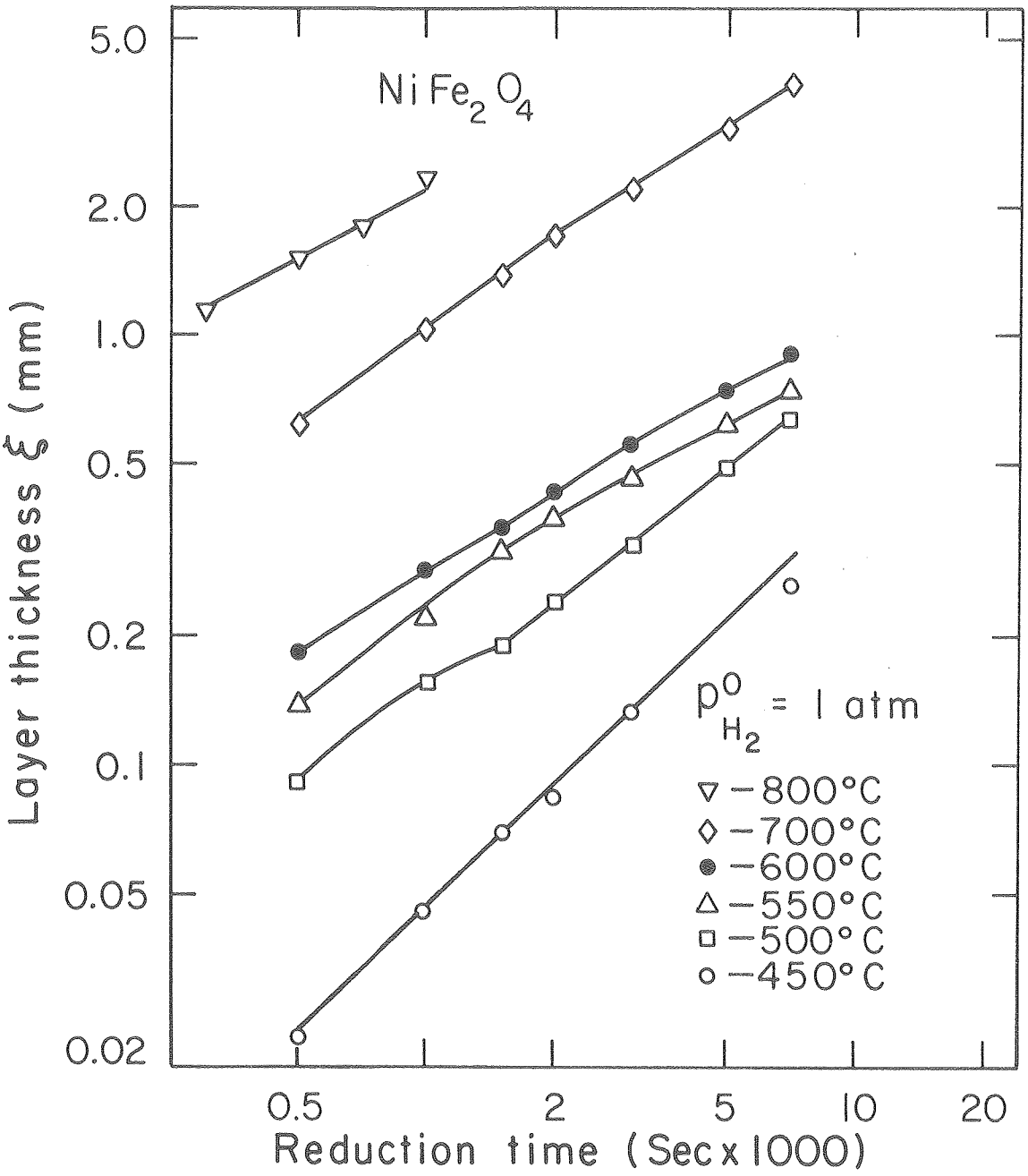

Figure 2

XBL 807-1525

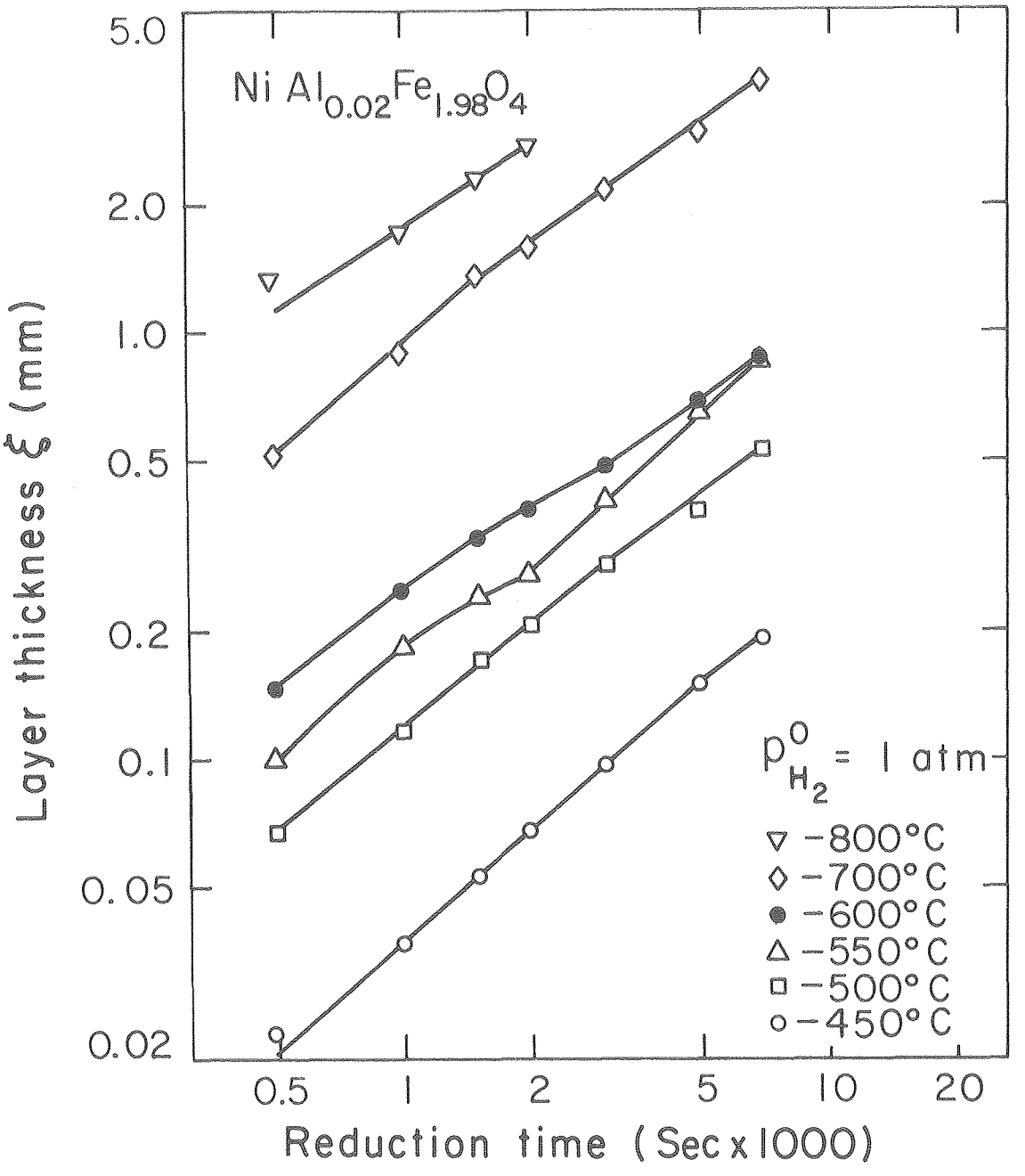

Figure 3

XBL 807-1521

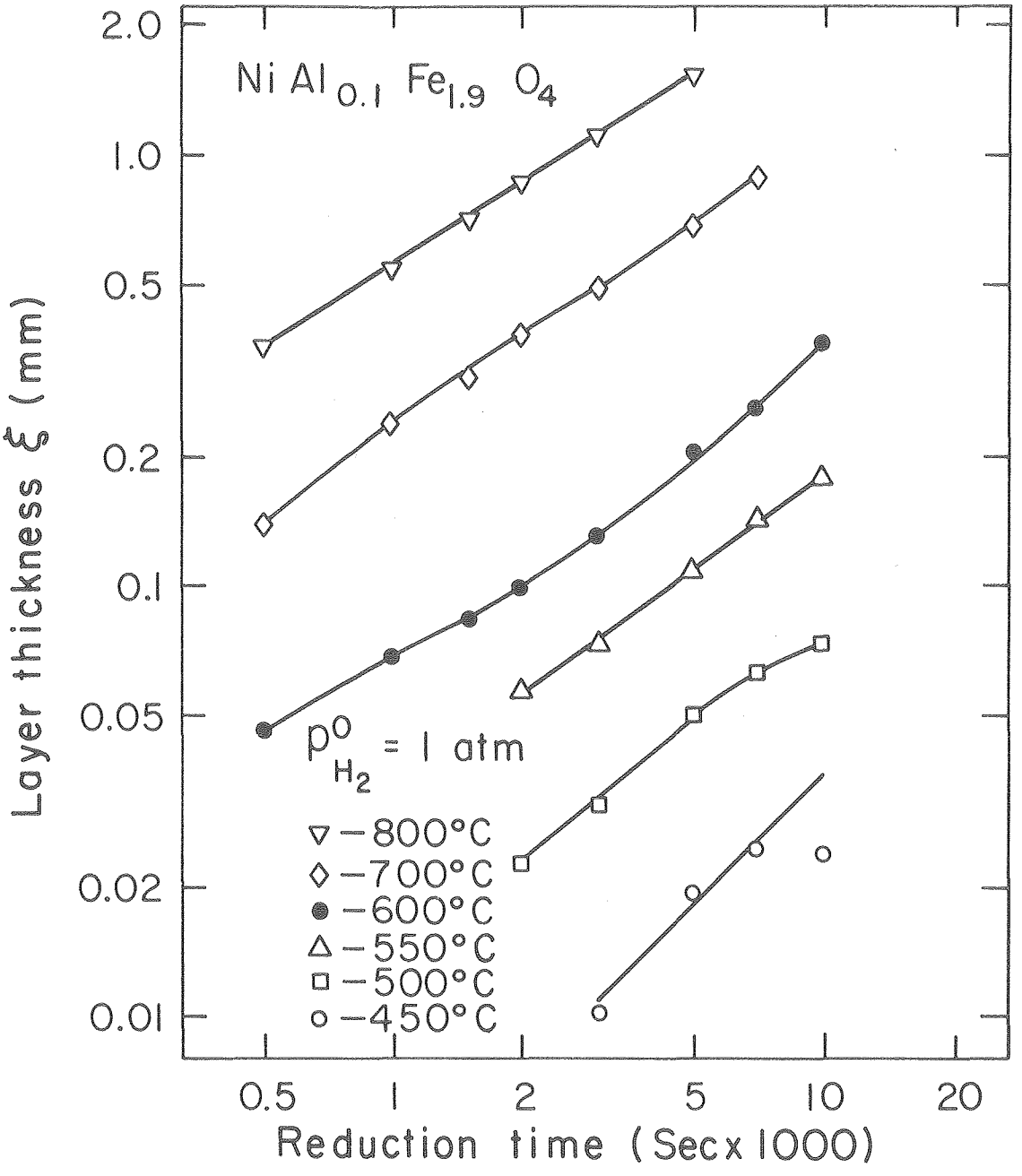

Figure 4

XBL807-1526

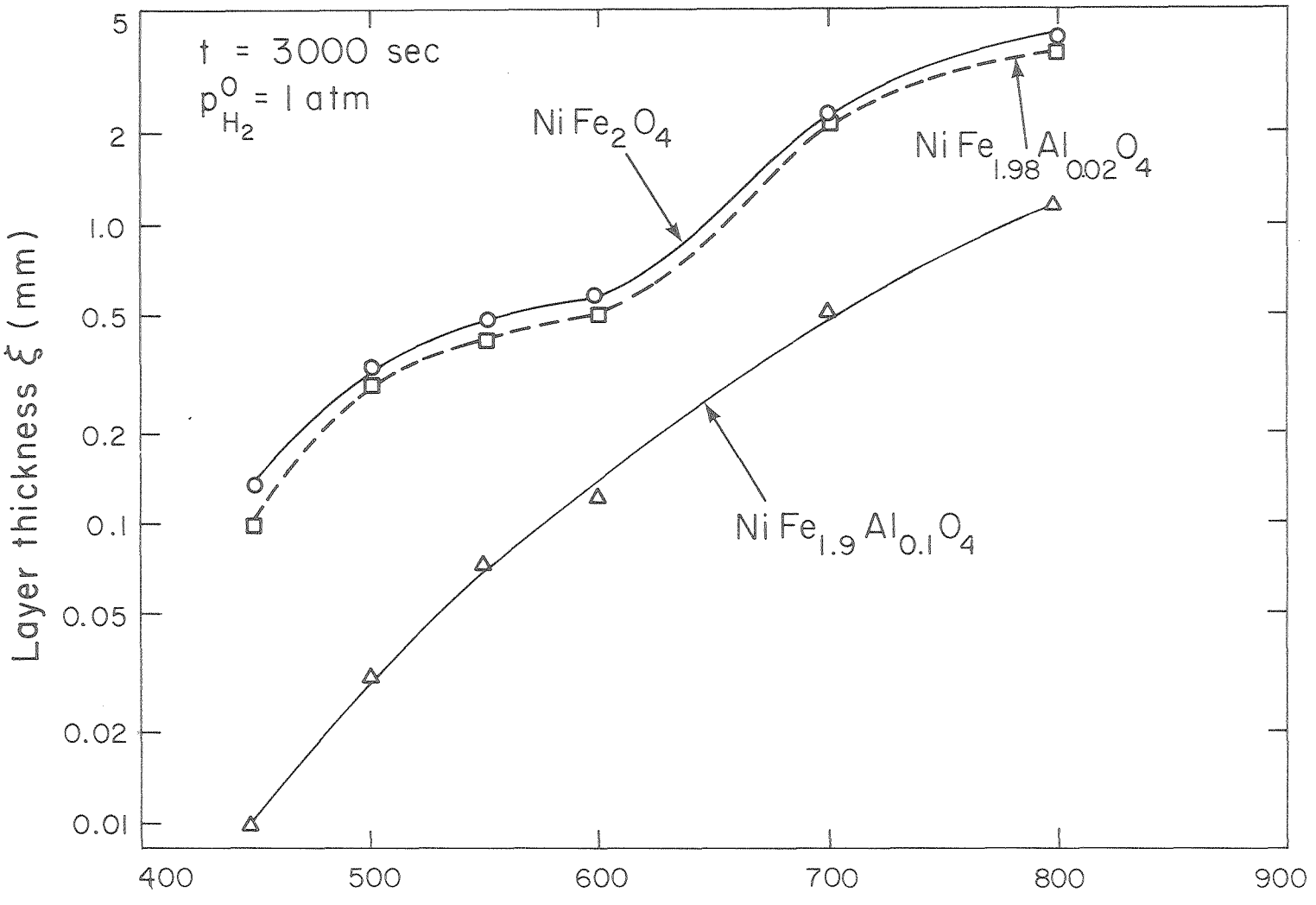

Figure 5

XBL 807-1527

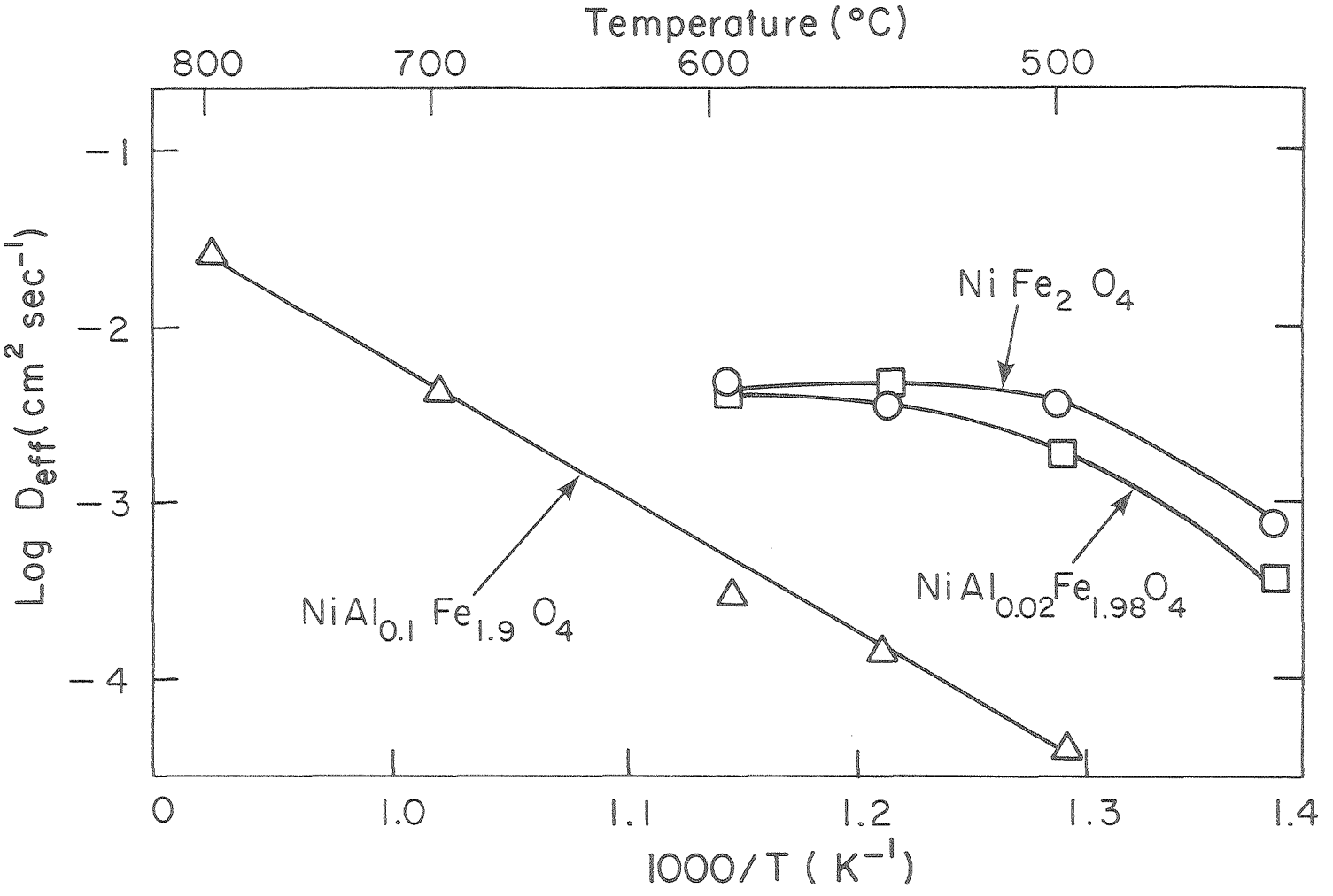

Figure 6

XBL807-1522

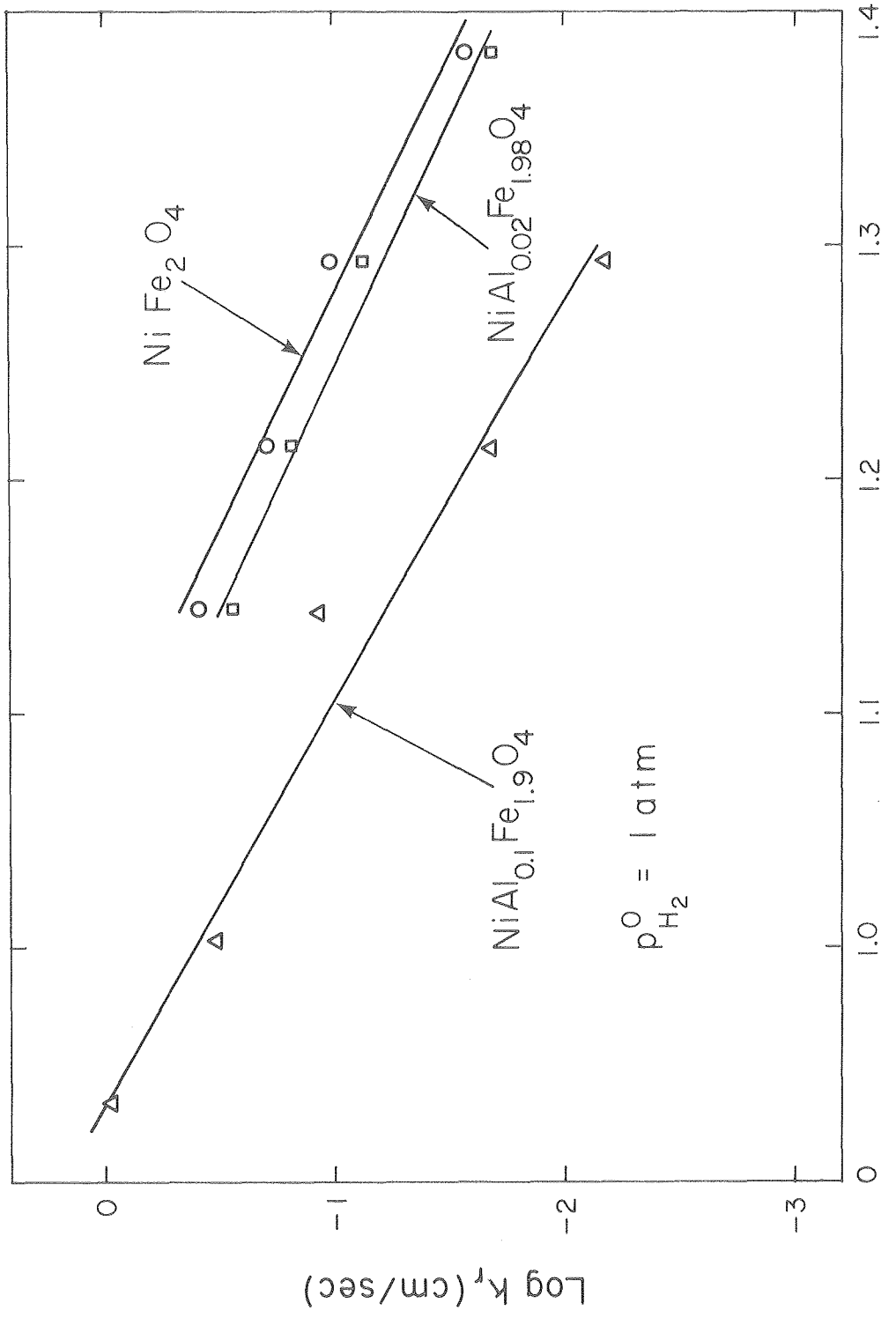

XBL807-1528

Figure 7

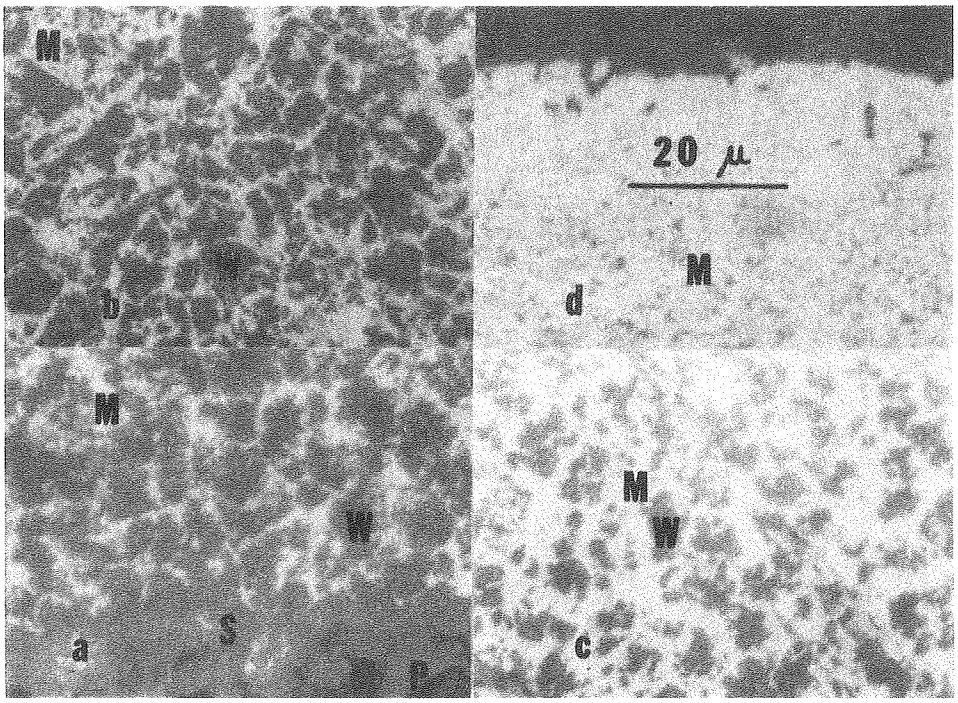

XBB 808-9666

Figure 8

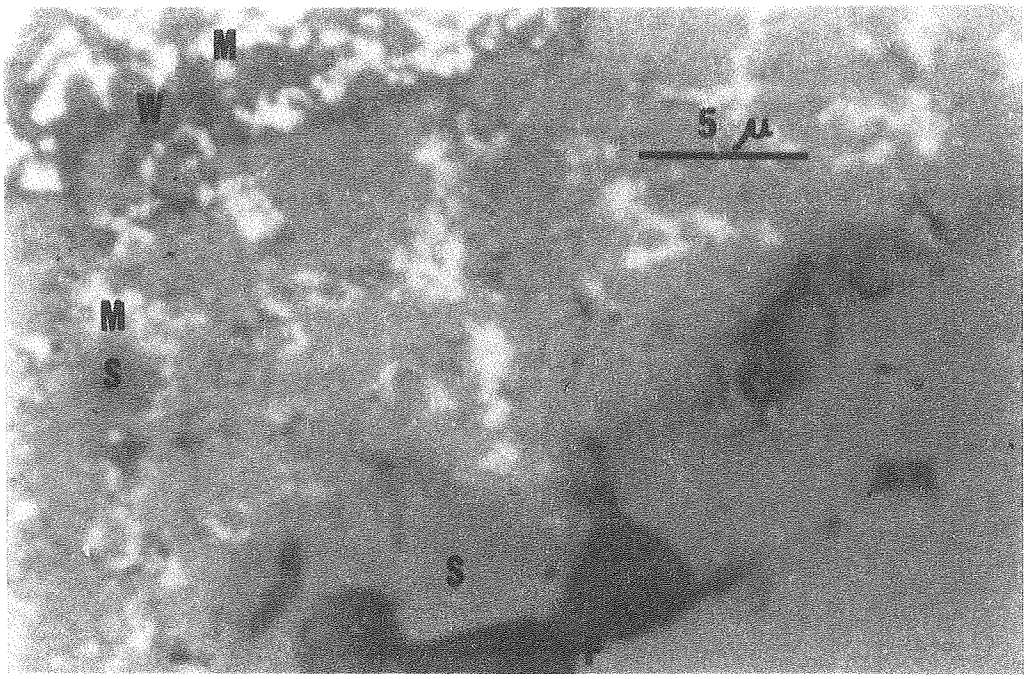

Figure 9

XBB 808-9663

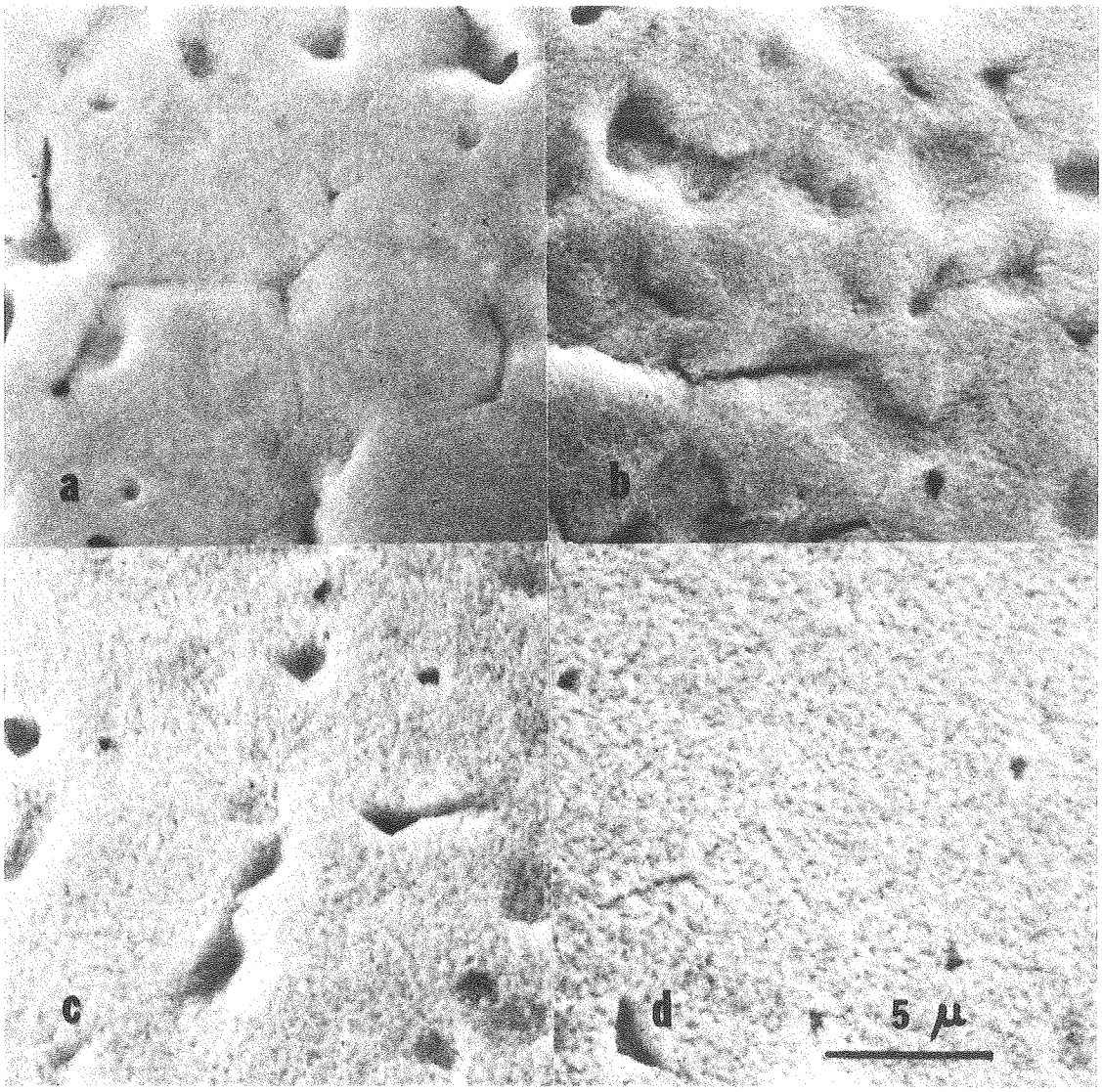

XBB 808-9665

Figure 10

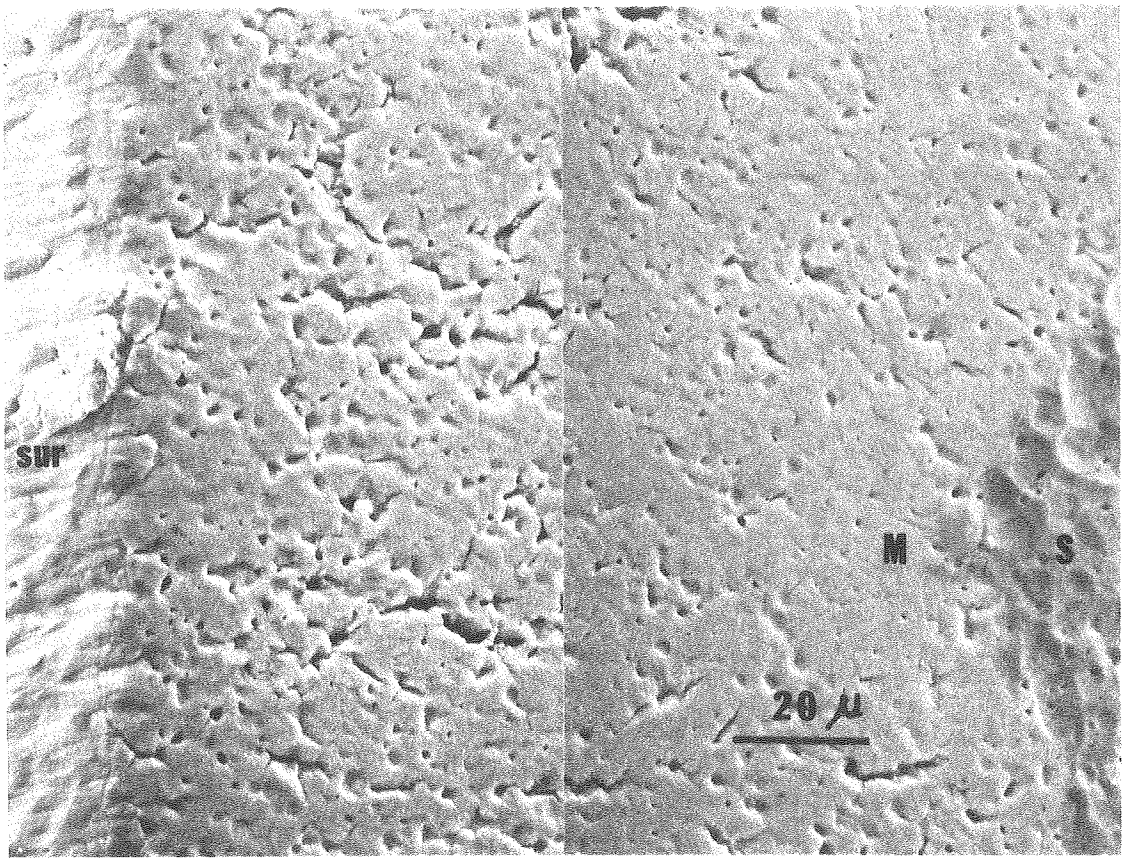

XBB 808-9664

Figure 11

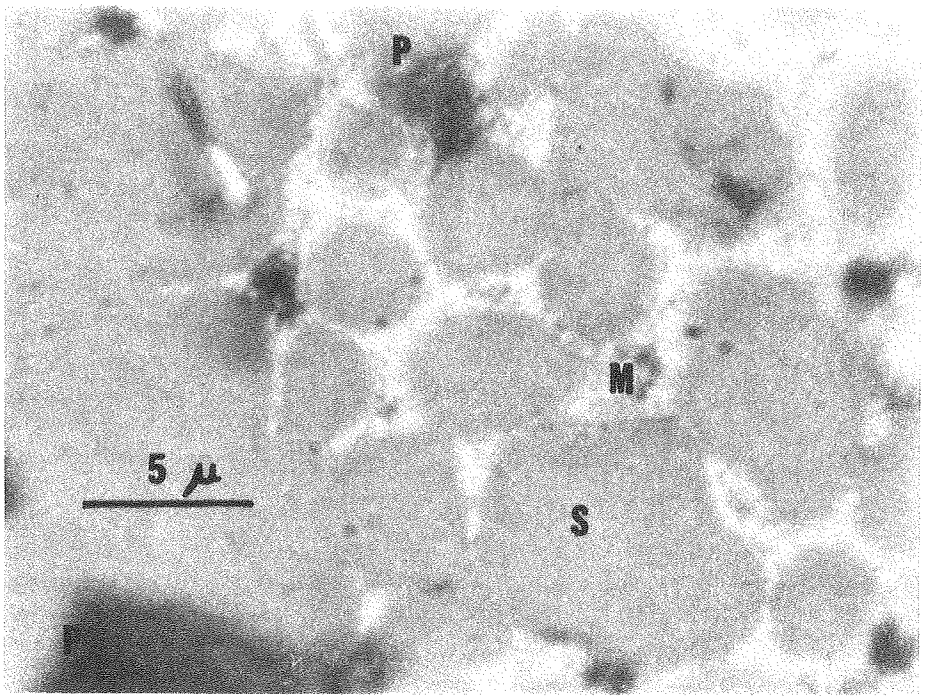

Figure 12

XBB 808-9667

TECHNICAL INFORMATION DEPARTMENT
LAWRENCE BERKELEY LABORATORY
UNIVERSITY OF CALIFORNIA
BERKELEY, CALIFORNIA 94720